Assessment of resting-state blood flow through anterior cerebral arteries by using transcranial Doppler recordings

Hanrui Huang, Ervin Sejdić*

Department of Electrical and Computer Engineering, University of Pittsburgh

Abstract

Transcranial Doppler (TCD) recordings are used to monitor cerebral blood flow in main cerebral arteries. The resting state is usually characterized by using the mean velocity or the maximum Doppler shift frequency (an envelope signal) by insonating the middle cerebral arteries (MCAs). In this study, we characterized the cerebral blood flow in the anterior cerebral arteries (ACAs). We analyzed both the envelope signals and the raw signals obtained from bilateral insonation. We recruited 20 healthy subjects and conducted the data acquisition for 15 minutes. Features were extracted from the time domain, the frequency domain and the time-frequency domain. The results showed that gender-based statistical difference exists in the frequency domain and the time-frequency domain. However, no handedness effect was found. In the time domain, the information-theoretic features showed that the mutual dependence is higher in raw signals than in envelope signals. Finally, we concluded that insonating the ACA will serve as a complement of the MCA studies. Additionally, the investigation of the raw signals provided us with additional information that is not otherwise available from the envelope signals. The direct TCD raw-data utilization is therefore validated as a valuable resting-state characterization method.

Keywords:
Transcrannial Doppler, anterior cerebral artery, resting-state characteristics.

*Ervin Sejdić is the corresponding author 412-624-0508 (3700 O'Hara Street Pittsburgh, PA, USA, 15261)
Email addresses: hah45@pitt.edu (Hanrui Huang), esejdic@ieee.org (Ervin Sejdić)

Introduction

Various imaging techniques, such as functional magnetic resonance imaging, positron emission tomography, and single photon emission computed tomography, have been used to study brain functions (Fransson, 2005), (Phelps et al., 1985), (Stroobant and Vingerhoets, 2000). In the past decades, the regional cerebral blood flow has been shown to be highly dependent on brain metabolism due to the need for O_2 and glucose (Deppe et al., 2004). Different from those typical imaging techniques, Transcranial Doppler (TCD), first introduced by Aaslid, Markwalder, and Nornes (Aaslid et al., 1982), allows for non-invasive investigation of cerebral blood flow with relatively high temporal resolution (Deppe et al., 2004). Researchers have taken advantage of the highly coupled relationship between the cerebral blood flow and brain activities to investigate human cognitive process (Fox and Raichle, 1986). Previous publications have successfully discussed the effect of gender (e.g., Matteis et al. (1998), Marinoni et al. (2009)) and age (e.g., Torbey et al. (2001)) on the cerebral blood flow velocity using TCD. There are several major advantages of TCD. First, it is inexpensive to acquire in comparison to other methods such as magnetic resonance imaging systems (Stroobant and Vingerhoets, 2000). Second, TCD is relatively simple to operate meaning that experimental data acquisition or clinic diagnosis of neurological disorders such as stroke (e.g., Ducrocq et al. (1998)) is easily achievable. Therefore, TCD has been seen as a promising and powerful tool in monitoring of brain activities. Recently, functional TCD monitoring was even proposed as an innovative way of building a brain-computer interface (Myrden et al., 2011), (Myrden et al., 2012).

TCD is an ultrasound-based medical imaging technique whose principle is the application of Doppler effect. It utilizes spectral estimation to find the Doppler frequency shift and accordingly estimates the cerebral blood flow velocity (CBFV). Assumptions of this technique include the estimation of the insonation angle, ideal modeling of the blood vessel, and modeling of blood particles' movement within (Azhari, 2010). However, TCD is currently constrained to only targeting large vessels (i.e. the main arteries)(Min et al., 2010).

There are three major cerebral arteries: middle cerebral artery (MCA), anterior cerebral artery (ACA) and posterior cerebral artery (PCA) (Stroobant and Vingerhoets, 2000). In many publications assessing cognitive tasks using fTCD (e.g., Carey et al. (2001), Droste et al. (1989), Hartje et al. (1994)), the MCA is mostly insonated as over 80% blood delivery to the brain is achieved through MCA (Stroobant and Vingerhoets, 2000). Also, cerebral blood flow through MCA is relatively easy to detect with the ultrasound probe due to the anatomical structure (Gibo et al., 1981). However, the ACA (60-75mm), which lies deeper than the MCA (35-60mm) (White and Venkatesh, 2006), delivers blood to frontal lobes and superior medial parietal lobes (Bradac, 2011). As these regions are involved in receptive language and episodic memories (Ross, 1980), (Alexander et al., 1989), (Wagner et al., 2005), insonating ACA data appears to be viable as a complemental method to solely using the MCA in understanding the resting-state characteristics of cerebral blood flow.

To properly characterize the resting-state cerebral blood flow, we are aiming to investigate features in multiple domains due to the complexity of human brain (Sporns et al., 2004). However, previous TCD studies only considered the so-called envelope signal (i.e., the peak values in the TCD spectrum, see Figure 1) (Kelley et al., 1992), (Stroobant et al., 2009), (Duschek and Schandry, 2003). By considering only the envelope signals, valuable information about cerebral blood flow characteristics may be lost. It is expected that the raw data (see Figure 2), used in calculation of the envelope signals, contains more comprehensive information about the resting-state characteristics. Following the previous study of the MCA resting-state characteristics (Sejdić et al., 2013), this paper presents a comparative study of cerebral blood flow in ACA using both the envelope signal and the raw data. To carry out the comparative analysis, we considered a range of features using classical and modern analysis tools.

Methodology

Subjects

The cerebral blood flow velocity data was collected from twenty healthy voluntary subjects, 9 males and 11 females. The subjects were first requested to read through and sign the consent form that has been approved by the University of Pittsburgh Institutional Review Board. None of the participants had a history of heart murmurs, strokes, concussions, migraines or any other brain or neurological conditions. Basic demographic information including age, height, and weight was also collected. Table 1 summarizes the demographic information of the consenting participants.

The handedness of each participant was assessed using the Edinburgh Handedness Inventory (Oldfield, 1971) before data acquisition, and the result was scored based on the formula below (Oldfield, 1971):

$$\text{Handedness Score} = \frac{\sum_{i=1}^{N} X(i,R) - \sum_{i=1}^{N} X(i,L)}{\sum_{i=1}^{N} X(i,R) + \sum_{i=1}^{N} X(i,L)} \tag{1}$$

where $X(i, L/R)$ is evaluated as either 1 (preferred) or 2 (dominant) for the left (right) hand doing certain activities. The subjects' scores are summarized in Table 2.

Procedure

Bilateral cerebral blood flow in the ACA was measured using a SONARA TCD system (CareFusion, San Diego, CA, USA) with two 2 MHz transducers placed on the transtemporal window through which the ultrasound can penetrate the skull and reach the arteries (Stroobant and Vingerhoets, 2000). Since the ACA and the MCA are anatomically close to each other (Gibo et al., 1981), the signal was obtained by slightly rotating the probes after the MCA signal was obtained. This adjustment could be nontrivial, but the blood flow from two arteries is easily distinguishable. The direction of the blood flow in the ACA is opposite to the blood flow in the MCA (Kelley et al., 1992). The depth of the ACA is about 10-15mm deeper than the MCA, which also serves as an indicator that the ACA has been successfully insonated.

The data acquisition lasted for 15 minutes for each participant. The participants were requested to keep quiet and as thought-free as possible during this process. The probes were fixed using an elastic headband to around 5 cm in front of the ears, above the zygomatic arch (Piechnik et al., 1999). The specific insonation location may vary depending on the signal intensity obtained by the TCD system from different subjects. The end-tidal carbon dioxide was monitored throughout the data acquisition using the BCI Capnocheck Sleep (Smiths Medical PM, Inc. Waukesha, Wisconsin, USA). The subjects were also fitted with sensors to record the electrocardiogram, respiration rate, skin conductance and head movement during the recordings. These sensors are part of a multisystem physiological data monitoring system made by Nexus-X (Mindmedia, Netherlands).

The raw data was extracted as audio files with a sampling frequency of 44100 Hz. They were downsampled by a factor of 5 to speed up the computation since the TCD system uses a low-pass filter which filters out the frequency components above the maximum scale value that we configured in advance.

Feature extraction

The non-parametric statistical hypothesis test Wilcoxon rank-sum test (DePuy et al., 2005) was used to infer about statistical differences. The analysis flow is shown in Figure 3.

Statistical feature

Three basic parameters widely used in statistics: standard deviation, skewness and kurtosis (Papoulis and Probability, 1991), were employed to characterize (e.g., Chauvy et al. (1998), Christopher and Christian (2005)) the ACA signal from the left channel (L-ACA) and the right channel (R-ACA), respectively. The cross-correlation between the L-ACA and R-ACA is also considered. The zero-lag value was calculated by selecting the maximum coefficient in the obtained sequences.

Information-theoretic feature

The information-theoretic features have been extensively utilized in the analysis of neurological analysis (e.g., Aboy et al. (2006), Porta et al. (2000)). The Lempel-Ziv complexity (Hu et al., 2006), conditional entropy (Porta et al., 2000) and cross-conditional entropy (Porta et al., 2000) have been used to measure the complexity and regularity of biomedical signals. They provide us with indices reflecting the signals from predictability and randomness point of views.

To calculate the Lempel-Ziv complexity, we first quantized the objective signal into 100 levels, so the signal X_n can be expressed as $[x_1,\ x_2\ ...\ x_n]$ in terms of the quantized levels. Then these points were grouped in blocks of a length of L, where L increases from 1 to n. Let $P_s(i,j)$ denote the block $[x_i,\ x_{i+1},\ ...\ x_j]$ for all $i < j$. Then for each L, we check if P_s has already appeared with previous i and j. If not, we put this block as one element into a set, V. Finally, let $c(n)$ denote the number of elements in the set V, i.e., the number of distinct parsed blocks P_s, and the LZC is then defined as follows:

$$LZC = \frac{c(n)(\log_{100} c(n) + 1)}{n} \tag{2}$$

To calculate the conditional entropy (CE), the process x_i is normalized and grouped in blocks of length L, $10 \leq L \leq 30$, such that $S_L(i) = [x(i), x(i-1), ...x(i-L+1)]$. CE is then calculated using the joint probability of the previous $L-1$ samples and their values (i.e., X_{L-1}) (Porta et al., 2000). Due to the underestimation of CE for larger L, (Porta et al., 2000) a corrective term, $perc(L)SE(1)$ was added to CE, where $SE(1)$ is the Shannon entropy (Coifman and Wickerhauser, 1992), and $perc(L)$ is the percentage of length L blocks found only once in the process. Then the regularity index is defined as:

$$\rho = 1 - min\left\{\frac{CE(L) + prec(L)SE(1)}{SE(1)}\right\} \tag{3}$$

Synchronization index (χ_{xy}) can be measured by extending and modifying the regularity index formula (Porta et al., 2000). Instead of making use of the previous $L-1$ samples in the self signal, x_{L-1}, we replace it with those of the synchronized signal, y_{L-1}. The joint probability thus involves the current $x(i)$ being looked at and the previous $L-1$ samples in y. The synchronization index is then defined as

$$\chi_{xy} = 1 - min\left\{\frac{CExy(L) + prec(L)SEy(1)}{SEy(1)}, \frac{CEyx(L) + prec(L)SEx(1)}{SEx(1)}\right\} \tag{4}$$

where $CE_{xy}(L)$ is the conditional entropy of the current x given the previous $L-1$ y sample points, and similarly, $CE_{yx}(L)$ denotes the conditional entropy of the current y given the previous $L-1$ x sample points.

Frequency analysis

In the frequency domain, the following parameters were utilized:

The peak frequency (f_p) is defined as the frequency which has the largest squared value in the frequency spectrum.

$$f_p = \text{argmax}_f \left\{|F_X(f)|^2\right\} \tag{5}$$

It measures the frequency value where the largest power occurs.

The centroid frequency (f_c) measures the center of frequency components in the spectrum taking center of mass as an analogy (Quan and Harris, 1997). It is defined as:

$$f_c = \frac{\int_0^{f_{max}} f|F_X(f)|^2 df}{\int_0^{f_{max}} |F_X(f)|^2 df} \tag{6}$$

The bandwidth (BW) of the spectrum is a measure of the spreadness of the frequency components (Li, 2000). It is defined as:

$$BW = \sqrt{\frac{\int_0^{f_{max}} (f - f_c)^2 |F_X(f)|^2 df}{\int_0^{f_{max}} |F_X(f)|^2 df}} \tag{7}$$

where F_X in (6) and (7) is the Fourier transform of the original signal, and the Fast Fourier Transform was used for computing these quantities.

Time-frequency analysis

The Meyer wavelet has infinite differentiability and good time-frequency localization and thus is popular in physiological signal processing (e.g., (Lee et al., 2010)). The corresponding relative energy and energy entropy were considered (Rosso et al., 2001).

The relative energy is defined as the ratio between the energy at the ith level (E_i) and the total energy (E_{total}). E_{total} is calculated as the Euclidean norm (Rosso et al., 2001), (Lee et al., 2010) of the vector $V = [a_{10}, d_{10}, d_9, ...d_1]$, where a_{10} denotes the approximation coefficient and d_i denotes the detail coefficient at the ith level (Bračič and Stefanovska, 1998), (Stanković et al., 2012). The mathematical expressions are:

$$E_{total} = \|V\| \tag{8}$$

$$E_a = \frac{a^2}{E_{total}} \tag{9}$$

$$E_{d_i} = \frac{d_i^2}{E_{total}} \tag{10}$$

The wavelet entropy can be regarded as a measure of how well the process behaves, or in other words, a measure of information distribution (Rosso et al., 2001).

$$WE = -\sum_i E \log_2 E \qquad (11)$$

where E is the relative energy calculated above in (8). A lower value of WE (close to 0) implies that the wavelet energy is relatively concentrated on a certain band. On the contrary, a more random process would result in a higher value of WE which represents the spreadness of the wavelet energy over many decomposed levels.

Results

To safely present the TCD measurement results, we firstly exclude the possibility that the features were influenced by the end-tidal carbon dioxide level (Giller et al., 1993). Firstly, by taking linear regression test, no evidence was found that the $ETCO_2$ level was affected by the body mass index for either gender. Secondly, we observed the trend of the CO_2 recording for every participant and found no dramatic fluctuation exists.

Statistical feature

A summary of statistical feature values for the envelope signals (mean $\pm$ standard deviation) is presented in Table 3. A high cross-correlation between the left and right ACA blood flow was obtained for all subjects. This was expected considering these signals generally synchronize due to the normal vasodilation and vasoconstruction. The standard deviation, which represents how far the sample data deviate from the mean, was found to be statistically higher in the female group than in the male group (R-ACA: $p = 0.04$; L-ACA: $p = 0.01$). This implies that the cerebral blood flow changes within a wider range in females than in males. The female group also has statistically higher skewness (R-ACA: $p = 0.04$; L-ACA $p = 0.03$) and kurtosis than the male group ($p < 0.05$ for both channels).

When comparing the left-handed group with the right-handed group, however, fairly high p-values for both channels (skewness: $p > 0.40$; kurtosis: $p > 0.68$) were obtained. That implies that the null hypothesis could not be rejected.

Similarly, the statistical feature for the raw signals are presented in Table 4. Unlike the results for the envelope signals, statistical difference between males and females was only found in the standard deviation values (R-ACA: $p < 0.01$; L-ACA: $p = 0.01$). Another major discrepancy is that the cross-correlation between the left channel and the right channel is relatively lower in the raw signal (≈ 0.01), which represents that the dependence in the raw signals is lower than that in the envelope signals.

Information-theoretic feature

The information-theoretic features of the envelope signal are presented in Table 5. The calculations of Lempel-Ziv complexity do not show any statistical difference on either channel between females and males ($p > 0.08$), nor between left-handed and right-handed ($p > 0.09$). The regularity index on both channels is low, but the synchronization is relatively higher. This implies that the signal is more predictable by looking at the opposite channel than looking at itself.

Table 6 shows the feature values of the raw signals. The mean values of Lempel-Ziv complexity (≈ 0.68) are similar to those calculated for the envelope signals. However, the raw signals have higher regularity than the envelope signal in the time domain ($p < 0.01$). The raw signals also have higher synchronization than the envelope signal ($p < 0.01$), which means the raw signals from the two channels contain more mutual information. In terms of the value of the regularity and synchronization index, neither gender-based ($p > 0.17$) nor handedness-based ($p > 0.13$) statistical difference was found.

Frequency domain feature

Table 7 summaries the features in the frequency domain of the envelope signals, and Table 8 summaries the features of the raw signals. The envelope signals have low frequencies around 11–14 Hz. The peak frequencies appeared to be person-specific since the standard deviation is high compared to its mean. No statistical difference between males and females or between right-handed and left-handed subjects could be concluded for any of these feature values ($p > 0.05$).

For the raw data, the center frequency for R-ACA was found to be statistically higher in the female group than in the male group ($p = 0.02$). Additionally, significant difference was found between males and females in bandwidth on both channels (R-ACA: $p < 0.01$; L-ACA: $p = 0.01$). Considering that two out of three left-handed subjects are females, we reconsidered the left-handed group with right-handed-females and found out that no handedness effect could be concluded so far ($p > 0.05$).

Time-frequency feature

The relative energy calculated based on the 10-level wavelet decomposition and the wavelet entropy are summarized and presented in Figure 4 and 5. When considering the gender effect, no statistical difference could be found just by investigating the envelope signal (Figure 4). However, statistical difference can be found by looking at the raw signals.

The features for the raw data are summarized in Figure 5. There were gender-based difference in left channel entropy ($p = 0.01$). On the right channel, the detail coefficients d_{10}, d_9 and d_7 are shown to have gender-based difference ($p = 0.01, 0.04$ and 0.04 respectively). On the left channel, statistical difference was found in a_{10} ($p = 0.22$) and d_{10} ($p = 0.01$).

Besides, when comparing the left-handed and the right-handed subjects, no statistical difference was found ($p > 0.08$ for all levels). This finding is the same as what we find in other extracted features, no statistical difference between the left-handed group and the right-handed group could be concluded.

Discussion

In this section, we discuss the effects of gender and handedness on the extracted features from both the raw and envelope CBFV signals.

Comparison between raw and envelope signals regarding gender and handedness effect

In the previous section, no evidence has been found of any handedness effect on CBFV in ACA, while gender-based differences were discovered. This difference (females>males) is found to coincide with the findings by Marinoni et al. (2009) using the MCA and considering the mean velocity.

The statistical analysis of the signals yielded several important results. Firstly, the difference in the the shape of the probability density function between males and females were discovered by comparing the calculated values of skewness and kurtosis. This finding demonstrates the significance of envelope signals from a statistical point of view. We can see that the envelope signals solely provide sufficient confidence in distinguishing males and females. Secondly, the maximum cross-correlation between the left channel and the right channel is close to 0 for the raw signals, implying that the signals obtained from two channels have low dependence in the time domain. On the contrary, the maximum cross-correlation coefficient value of the envelope signals is high, implying that the envelope signals have a high similarity at zero-lag between the two channels in the time domain. Considering that the mean velocity is a direct reflection of the cerebral blood flow under certain strict assumptions, we believe the high correlation is obtained due to the loss of information carried by blood cells at lower speed in the arteries, which has never been considered in clinical application or any other research. Handedness wise, however, none of these obtained features is found to exhibit any handedness effect.

From the information-theoretic point of view, the results show that the amount of information is not affected by gender or handedness. Interestingly, the envelope signals have almost the same Lempel-Ziv complexity as the raw signals. Despite the absence of statistical evidence depicting major differences, its clinical significance underlies its role as an indicant of brain function complexity (Wu and Xu, 1991) and brain information transmission (Xu et al., 1997) as a metric to estimate the complexity of descrete-time physiologic signals. Similarly, however, the envelope signals produce a low regularity index (close to 0), while the raw signals have a higher one. This means that the raw signals are actually more predictable than the envelope signals which are continuously used for clinical purposes.

In the frequency analysis, the raw signals contain higher frequency components than do the envelope signals. In fact, the time domain features of the envelope signal already reflects some frequency domain characteristics because the calculation that yields envelope signals involves short-time Fourier transform (Deppe et al., 2004). Comparatively, the frequency analysis quantifies several parametric values in the frequency domain, while the time domain analysis of the envelope signal only provides a simple summary about the shape of the probability density function. Also, more specific features were found in the frequency analysis. Firstly, the envelope signals have a low-pass characteristic while the raw signals have a band-pass characteristic. This result is consistent with most physiological signal analysis such as electrocardiogram (ECG) signals (0.5 - 40 Hz) (Thakor and Zhu, 1991). Secondly, we noticed that large standard deviation values were obtained for the peak frequency feature when considering the envelope signals. This implies that metabolic differences exist between individuals and that the peak frequency of the envelope signals is not necessarily the most robust feature of these signals. Fortunately, the raw signal has a relatively more concentrated peak frequency statistic for both females and males. Additionally, the seeming differences between left-handed and right-handed subjects were found to be resulted from the gender effect rather than the handedness effect. That is to say, although gender effect has been clearly found out, handedness was not an obvious parameter that contributes to the frequency domain differences. On the other hand, the low-pass characteristic of the envelope signal is more likely to be contaminated by other physiological artifacts and the raw data avoids this disadvantage.

The time-frequency analysis has further demonstrated the existence of gender-based difference. A possible clinical application could be the signal change detection (Li et al., 1995). Some of the detail coefficients calculated from the raw signal have shown significant difference between males and females. Comparatively, the envelope signal only shows that about 93% energy are concentrated around the approximate coefficient, i.e., the low time-frequency band. Otherwise, no handedness effect was found.

Utilization of raw data and ACA signals

Instead of only considering the envelope signal or the mean BFV, we also directly used the raw data to characterize the TCD measurements. This will be particularly important in future studies when cerebral blood flow during cognitive tasks is considered. In this study, we established the resting-state characterization using both the envelope and raw signals. Our study has shown that the raw data contains information that we could not capture by simply looking at the envelope signals.

Despite that the MCA was insonated in most of the related studies, we hope to characterize the cerebral blood flow using the ACA in addition to the MCA. Comparing with our previous MCA study (Sejdić et al., 2013), we have found out that in the frequency domain, the bandwidth of the ACA signals is larger than that of the MCA signals. The ACA has $\approx$ 13 Hz in envelope signals and $\approx$ 600 Hz in raw signals, while the MCA has $\approx$ 10 Hz in envelope signals and $\approx$ 500 Hz in raw signals. Bandwidth difference between the ACA and the MCA indicates different cut-off frequencies and hence represents different frequency response characteristics. In the time-frequency domain, the wavelet entropy calculation is also found to be presenting statistical difference. MCA has wavelet entropy at 1.77 ± 0.17 (Sejdić et al., 2013), and ACA has 1.94 ± 0.16. This finding demonstrates a different energy spreadness over different levels. On the other hand, there also exists consistency in our current ACA study and the previous MCA study. Firstly, in both the MCA and the ACA analysis, the time domain features of envelope and raw signals have exhibited similar results in kurtosis, skewness and cross-correlation. This demonstrates the similarity between the shapes of the probability density function considered in the ACA and the MCA. Secondly, in the frequency domain, the MCA and the ACA have similar findings in peak and centroid frequencies. Lastly, in the time-frequency domain, when considering the raw signal, most energy concentrates around the 8th level and spreads over neighboring levels in both the ACA and the MCA.

Conclusions

In this study, we investigated the resting-state characteristics of cerebral blood flow through anterior cerebral arteries using the transcranial Doppler recordings. We collected data from 20 healthy participants during a 15-minute resting period. Both the envelope signals and the raw TCD signals were considered. The acquired data was analyzed in time, frequency and time-frequency domain. The results of the numerical analysis showed several important trends. In the time domain, we have found that the envelope signals carries good amount of representative features in terms of the separation of males and females, and hence it is sufficient to use envelope signal in this sense. In the information-theoretic analysis, the envelope signals and the raw signals are found to contain almost the same amount of information except the raw signals have higher synchronization. In the frequency domain, the envelope signals exhibited a low-pass characteristic, while the raw signals exhibited a band-pass characteristic. We may thus take advantage of the band-pass characteristic in the future to avoid other low-frequency physiological artifacts. Finally, the time-frequency features were extracted using 10-level Mayer discrete wavelet decomposition. They have shown that the energy of the envelope signals are concentrated on the low frequency band while the energy of the raw signals are more spread out in several bands. We have found statistical differences between males and females in the time, frequency and time-frequency domain. However, no handedness effect could be concluded.

Acknowledgement

The authors would like to express the greatest gratitude to all the participants who have supported me throughout the data collection.

References

Aaslid R, Markwalder T, Nornes H. Noninvasive transcranial Doppler ultrasound recording of flow velocity in basal cerebral arteries. Journal of Neurosurgery, 1982;576:769–774.

Aboy M, Hornero R, Abasolo D, Alvarez D. Interpretation of the Lempel-Ziv Complexity Measure in the Context of Biomedical Signal Analysis. IEEE Transactions on Biomedical Engineering, 2006;5311:2282 –2288.

Alexander M, Benson D, Stuss D. Frontal lobes and language. Brain and Language, 1989;374:656–691.

Azhari H. Basics of biomedical ultrasound for engineers. Wiley-IEEE Press, 2010.

Bračič M, Stefanovska A. Wavelet-based analysis of human blood-flow dynamics. Bulletin of Mathematical Biology, 1998;605:919–935.

Bradac G. Anterior Cerebral Artery. Cerebral Angiography, 2011:47–56.

Carey B, Manktelow B, Panerai R, Potter J. Cerebral autoregulatory responses to head-up tilt in normal subjects and patients with recurrent vasovagal syncope. Circulation, 2001;1048:898–902.

Chauvy P, Madore C, Landolt D. Variable length scale analysis of surface topography: characterization of titanium surfaces for biomedical applications. Surface and Coatings Technology, 1998;1101:48–56.

Christopher JJ, Christian WH. Independent component analysis for biomedical signals. Physiological Measurement, 2005;261:R15.

Coifman R, Wickerhauser M. Entropy-based algorithms for best basis selection. IEEE Transactions on Information Theory, 1992;382:713–718.

Deppe M, Ringelstein E, Knecht S. The investigation of functional brain lateralization by transcranial Doppler sonography. NeuroImage, 2004;213:1124–1146.

DePuy V, Berger V, Zhou Y. Wilcoxon–Mann–Whitney Test. Encyclopedia of Statistics in Behavioral Science, 2005.

Droste D, Harders A, Rastogi E. A transcranial doppler study of blood flow velocity in the middle cerebral arteries performed at rest and during mental activities. Stroke, 1989;208:1005–1011.

Ducrocq X, Hassler W, Moritake K, Newell D, von Reutern G, Shiogai T, Smith R. Consensus opinion on diagnosis of cerebral circulatory arrest using Doppler-sonography: Task Force Group on cerebral death of the Neurosonolgy Research Group of the World Federation of Neurology. Journal of the Neurological Sciences, 1998;1592:145–150.

Duschek S, Schandry R. Functional transcranial Doppler sonography as a tool in psychophysiological research. Psychophysiology, 2003;403:436–454.

Fox P, Raichle M. Focal physiological uncoupling of cerebral blood flow and oxidative metabolism during somatosensory stimulation in human subjects. Proceedings of the National Academy of Sciences, 1986;834:1140–1144.

Fransson P. Spontaneous low-frequency BOLD signal fluctuations: An fMRI investigation of the resting-state default mode of brain function hypothesis. Human Brain Mapping, 2005;261:15–29.

Gibo H, Carver C, Rhoton Jr A, Lenkey C, Mitchell R. Microsurgical anatomy of the middle cerebral artery. Journal of Neurosurgery, 1981;542:151–169.

Giller C, Bowman G, Dyer H, Mootz L, Krippner W. Cerebral arterial diameters during changes in blood pressure and carbon dioxide during craniotomy. Neurosurgery, 1993;325:737–742.

Hartje W, Ringelstein E, Kistinger B, Fabianek D, Willmes K. Transcranial doppler ultrasonic assessment of middle cerebral artery blood flow velocity changes during verbal and visuospatial cognitive tasks. Neuropsychologia, 1994;3212:1443–1452.

Hu J, Gao J, Principe J. Analysis of biomedical signals by the Lempel-Ziv complexity: the effect of finite data size. IEEE Transactions on Biomedical Engineering, 2006;5312:2606–2609.

Kelley R, Chang J, Scheinman N, Levin B, Duncan R, Lee S. Transcranial Doppler assessment of cerebral flow velocity during cognitive tasks. Stroke, 1992;231:9–14.

Lee J, Sejdić E, Steele C, Chau T. Effects of liquid stimuli on dual-axis swallowing accelerometry signals in a healthy population. Biomedical Engineering Online, 2010;91:7.

Li C, Zheng C, Tai C. Detection of ECG characteristic points using wavelet transforms. IEEE Transactions on Biomedical Engineering, 1995;421:21–28.

Li S. Content-based audio classification and retrieval using the nearest feature line method. IEEE Transactions on Speech and Audio Processing, 2000;85:619–625.

Marinoni M, Ginanneschi A, Inzitari D, Mugnai S, Amaducci L. Sex-related differences in human cerebral hemodynamics. Acta Neurologica Scandinavica, 2009;975:324–327.

Matteis M, Troisi E, Monaldo B, Caltagirone C, Silvestrini M. Age and sex differences in Cerebral Hemodynamics: a transcranial Doppler Study. Stroke, 1998;295:963–967.

Min B, Marzelli M, Yoo S. Neuroimaging-based approaches in the brain-computer interface. Trends in Biotechnology, 2010;2811:552–560.

Myrden A, Kushki A, Sejdić E, Chau T. Towards increased data transmission rate for a three-class metabolic brain-computer interface based on transcranial Doppler ultrasound. Neuroscience Letters, 2012;5282:99–103.

Myrden AJB, Kushki A, Sejdić E, Guerguerian AM, Chau T. A brain-computer interface based on bilateral transcranial Doppler ultrasound. PLoS ONE, 2011;69:e24170–1–8.

Oldfield R. The assessment and analysis of handedness: the Edinburgh inventory. Neuropsychologia, 1971;91:97–113.

Papoulis A, Probability R. Stochastic processes. Vol. 3. McGraw-hill New York, 1991.

Phelps M, Mazziotta J, et al. Positron emission tomography: Human brain function and biochemistry. Science, 1985;2284701:799.

Piechnik S, Yang X, Czosnyka M, Smielewski P, Fletcher S, Jones A, Pickard J. The continuous assessment of cerebrovascular reactivity: a validation of the method in healthy volunteers. Anesthesia and Analgesia, 1999;894:944–944.

Porta A, Guzzetti S, Montano N, Pagani M, Somers V, Malliani A, Baselli G, Cerutti S. Information domain analysis of cardiovascular variability signals: evaluation of regularity, synchronisation and co-ordination. Medical and Biological Engineering and Computing, 2000;382:180–188.

Quan Y, Harris J. Seismic attenuation tomography using the frequency shift method. Geophysics, 1997;623:895–905.

Ross E. Left medial parietal lobe and receptive language functions mixed transcortical aphasia after left antmior cerebral artery infarction. Neurology, 1980;302:144–144.

Rosso O, Blanco S, Yordanova J, Kolev V, Figliola A, Schurmann M, Basar E. Wavelet entropy: a new tool for analysis of short duration brain electrical signals. Journal of Neuroscience Methods, 2001;1051:65–76.

Sejdić E, Kalika D, Czarnek N. An analysis of resting-state functional transcranial Doppler recordings from middle cerebral arteries. PLoS ONE, 2013;82:e55405–1–9.

Sporns O, Chialvo D, Kaiser M, Hilgetag C, et al. Organization, development and function of complex brain networks. Trends in Cognitive Sciences, 2004;89:418–425.

Stanković S, Orović I, Sejdić E. Multimedia Signals and Systems. Springer US, New York, NY, 2012.

Stroobant N, Buijs D, Vingerhoets G. Variation in brain lateralization during various language tasks: A functional transcranial Doppler study. Behavioural Brain Research, 2009;1992:190–196.

Stroobant N, Vingerhoets G. Transcranial Doppler ultrasonography monitoring of cerebral hemodynamics during performance of cognitive tasks: a review. Neuropsychology Review, 2000;104:213–231.

Thakor NV, Zhu YS. Applications of adaptive filtering to ECG analysis: noise cancellation and arrhythmia detection. IEEE Transactions on Biomedical Engineering, 1991;388:785–794.

Torbey M, Hauser T, Bhardwaj A, Williams M, Ulatowski J, Mirski M, Razumovsky A. Effect of age on cerebral blood flow velocity and incidence of vasospasm after aneurysmal subarachnoid hemorrhage. Stroke, 2001;329:2005–2011.

Wagner A, Shannon B, Kahn I, Buckner R. Parietal lobe contributions to episodic memory retrieval. Trends in Cognitive Sciences, 2005;99:445–453.

White H, Venkatesh B. Applications of transcranial Doppler in the ICU: a review. Intensive Care Medicine, 2006;327:981–994.

Wu X, Xu J. Complexity and brain function. Acta Biophysica Sinica, 1991;7:103–106.

Xu J, Liu R, Yang Q. Information transformation inhuman cerebral cortex. Physica D, 1997;106:363–374.

Tables

Table 1: Participants' demographic information

Distribution	Male	Female	Overall
Age	22.3 ± 1.64 years old	22.0 ± 2.00 years old	22.1 ± 1.86 years old
Height	180 ± 7.26 cm	163 ± 5.39 cm	171 ± 10.1 cm
Weight	91.6 ± 29.3 kg	52.6 ± 5.89 kg	68.9 ± 27.3 kg

Table 2: Participants' handedness distribution

	Right-handed	Left-handed	Bidextrous
Number of subjects	16	3	1
Gender	8 males	2 females	1 female
Average score	64	-63	0

Table 3 Statistical features for the envelope signals

	Male	Female	Left-handed	Right-handed
$Standarddeviation R$	11.4 ± 2.48	16.0 ± 4.18	17.7 ± 4.64	13.3 ± 3.75
$Standarddeviation L$	11.1 ± 3.06	18.2 ± 6.19	17.7 ± 4.61	14.6 ± 6.28
$Skewness R$	1.73 ± 1.04	0.90 ± 0.64	0.96 ± 0.09	1.33 ± 1.01
$Skewness L$	1.33 ± 0.49	0.85 ± 0.46	1.07 ± 0.42	1.06 ± 0.55
$Kurtosis R$	8.81 ± 7.57	4.54 ± 2.44	3.87 ± 0.61	6.92 ± 6.17
$Kurtosis L$	6.31 ± 2.84	3.98 ± 1.47	4.19 ± 1.37	5.18 ± 2.60
$Crosscorrelation$	0.93 ± 0.04	0.90 ± 0.05	0.88 ± 0.05	0.92 ± 0.88

Table 4: Statistical features for the raw signals. * denotes multiplication by 10^{-3}.

	Male	Female	Left-handed	Right-handed
$Standarddeviation R$	0.15 ± 0.04	0.10 ± 0.02	0.09 ± 0.02	0.13 ± 0.04
$Standarddeviation L$	0.14 ± 0.01	0.09 ± 0.02	0.09 ± 0.01	0.12 ± 0.05
$Skewness R$	$(-0.50 \pm 5.42)^*$	$(-1.94 \pm 8.84)^*$	$(-0.19 \pm 2.71)^*$	$(0.12 \pm 5.08)^*$
$Skewness L$	$(-0.10 \pm 2.54)^*$	$(2.06 \pm 8.70)^*$	$(7.08 \pm 10.1)^*$	$(-0.76 \pm 4.41)^*$
$Kurtosis R$	3.49 ± 0.49	3.87 ± 1.65	3.45 ± 0.56	3.46 ± 0.74
$Kurtosis L$	3.33 ± 0.33	4.41 ± 3.18	3.69 ± 0.92	3.32 ± 0.31
$Crosscorrelation$	0.01 ± 0.01	$(3.18 \pm 1.67)^*$	$(2.80 \pm 1.27)^*$	$(5.12 \pm 8.65)^*$

Table 5: A summary of information-theoretic features for the envelope signals. * denotes multiplication by 10^{-3}.

	Male	Female	Right-handed	Left-handed
$LZCR$	0.65 ± 0.04	0.68 ± 0.04	0.66 ± 0.04	0.70 ± 0.01
$LZCL$	0.67 ± 0.03	0.70 ± 0.03	0.70 ± 0.04	0.69 ± 0.01
$RegularityindexR$	0.08 ± 0.07	0.04 ± 0.05	0.07 ± 0.06	$(9.63 \pm 4.58)^*$
$RegularityindexL$	0.04 ± 0.04	0.03 ± 0.04	0.04 ± 0.04	0.02 ± 0.01
$Synchronization$	0.15 ± 0.07	0.13 ± 0.08	0.15 ± 0.08	0.09 ± 0.04

Table 6: A summary of information-theoretic features for the raw signals

	Male	Female	Right-handed	Left-handed
$LZCR$	0.68 ± 0.03	0.70 ± 0.03	0.69 ± 0.03	0.70 ± 0.02
$LZCL$	0.68 ± 0.03	0.68 ± 0.05	0.69 ± 0.03	0.68 ± 0.05
$RegularityIndexR$	0.38 ± 0.17	0.25 ± 0.15	0.30 ± 0.16	0.22 ± 0.14
$RegularityindexL$	0.37 ± 0.15	0.31 ± 0.25	0.31 ± 0.18	0.34 ± 0.27
$Synchronization$	0.37 ± 0.17	0.27 ± 0.19	0.30 ± 0.17	0.27 ± 0.15

Table 7: Frequency domain features for the envelope signals. * denotes multiplication by 10^{-3}.

	Male	Female	Right-handed	Left-handed
$Centroid frequency R$	11.9 ± 4.79	14.9 ± 4.02	12.9 ± 4.49	17.5 ± 3.34
$Centroid frequency L$	11.7 ± 3.74	15.6 ± 3.89	13.7 ± 4.14	14.4 ± 5.07
$Peak frequency R$	0.69 ± 0.51	0.42 ± 0.55	0.64 ± 0.55	$(4.41 \pm 5.42)^*$
$Peak frequency L$	0.57 ± 0.50	0.32 ± 0.52	0.51 ± 0.54	$(2.97 \pm 3.02)^*$
$Bandwidth R$	12.6 ± 2.52	13.9 ± 1.00	13.2 ± 2.08	14.2 ± 0.16
$Bandwidth L$	12.9 ± 1.54	13.9 ± 1.09	13.5 ± 1.38	13.5 ± 1.53

Table 8: A summary of frequency domain features for the raw signals

	Male	Female	Right-handed	Left-handed
$Centroid frequency R$	855 ± 198	1090 ± 197	979 ± 239	1060 ± 183
$Centroid frequency L$	850 ± 201	1060 ± 207	961 ± 232	1050 ± 209
$Peak frequency R$	523 ± 206	631 ± 259	603 ± 212	642 ± 241
$Peak frequency L$	526 ± 168	723 ± 543	526 ± 162	628 ± 107
$Bandwidth R$	627 ± 90.4	743 ± 81.5	682 ± 102	735 ± 114
$Bandwidth L$	606 ± 106	768 ± 129	694 ± 149	701 ± 139

Figures

Figure 1: A sample envelope signal

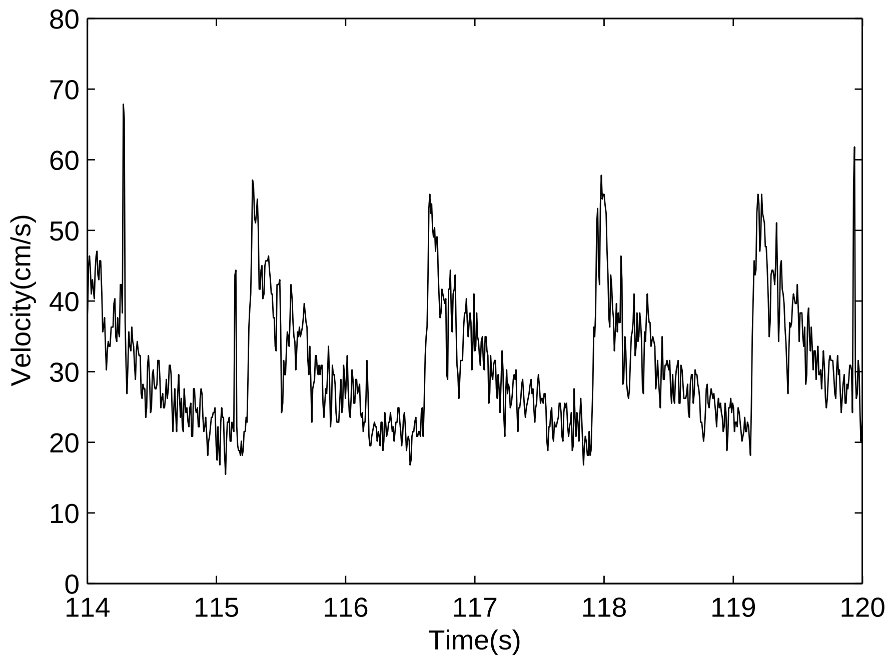

466 **Figure 2:** A sample raw signal

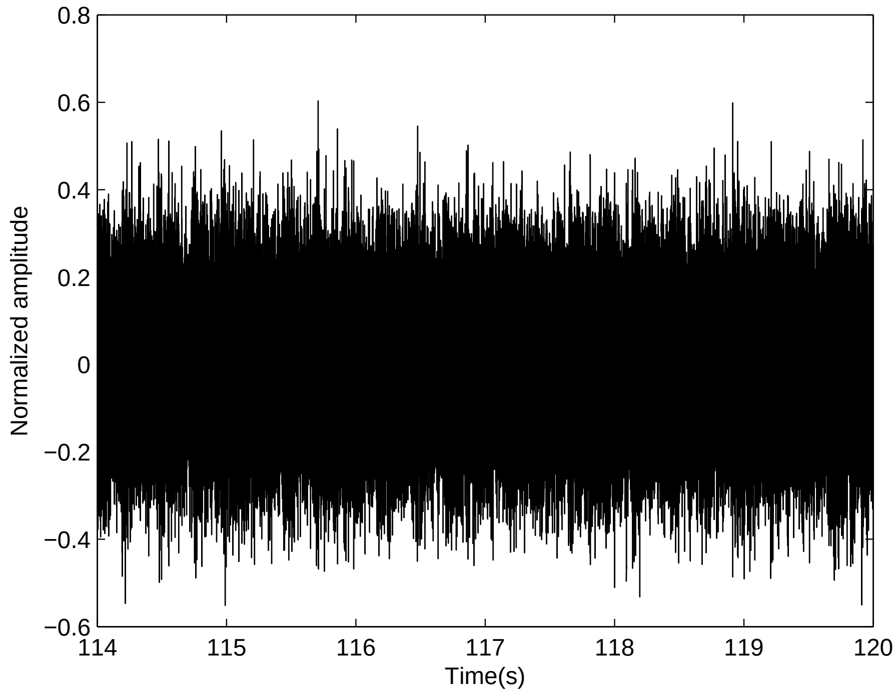

467 **Figure 3:** A feature extraction process implemented in this manuscript

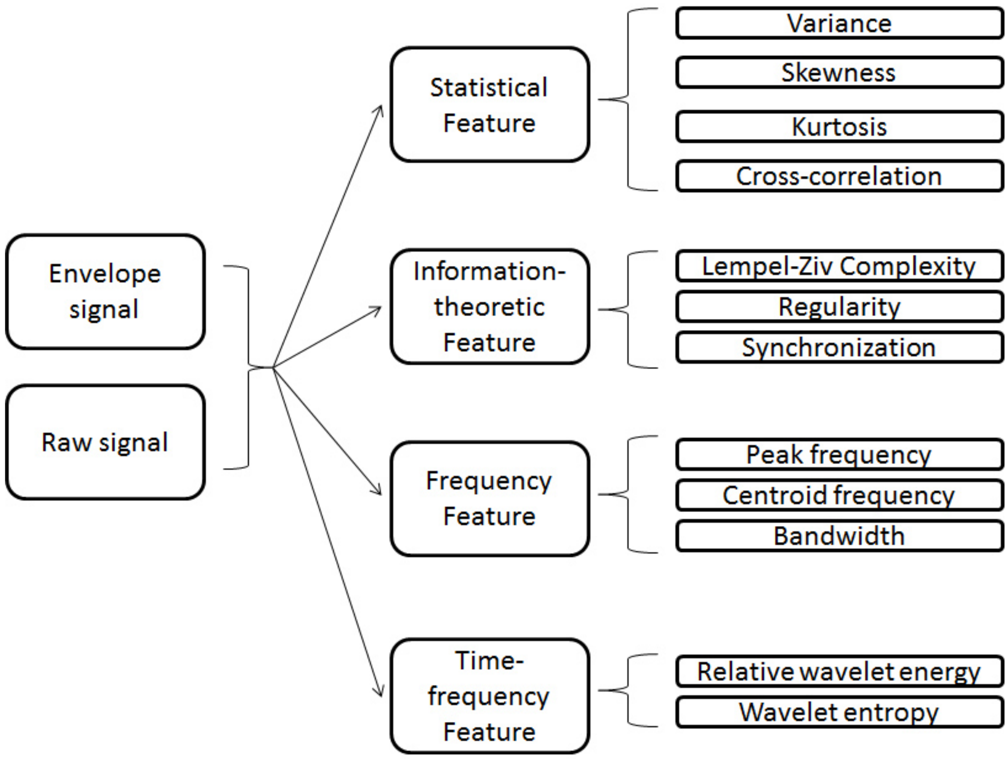

Figure 4: The 10-th level wavelet decomposition of envelope signals

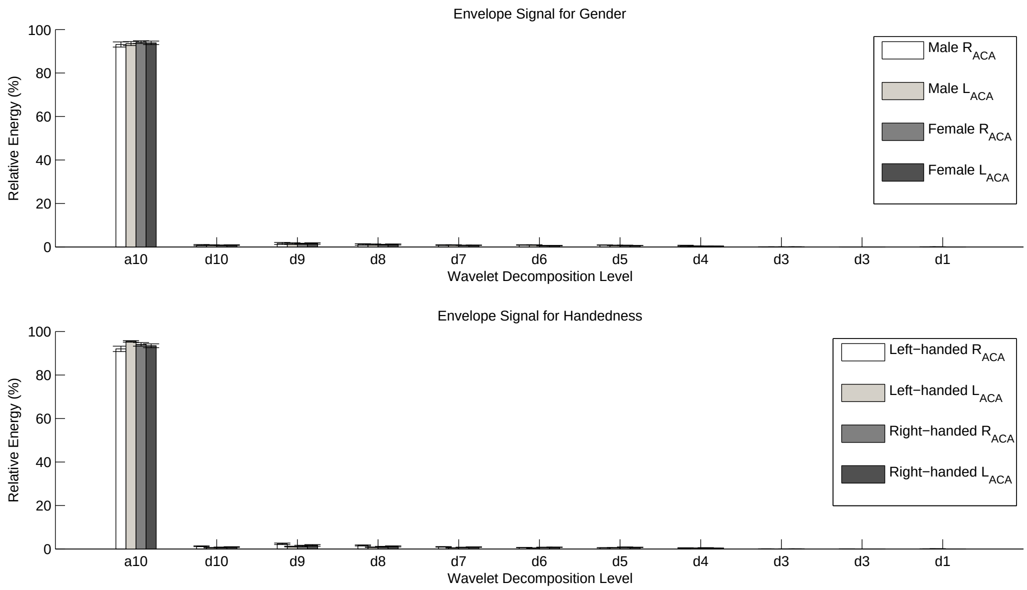

Figure 5: The 10-th level wavelet decomposition of raw signals